Hydrophobic Cr–Si mixed oxides as a catalyst for visible light-induced partial oxidation of cyclohexane†

Yasuhiro Shiraishi,* Hiroshi Ohara and Takayuki Hirai

Received (in Montpellier, France) 2nd June 2010, Accepted 26th July 2010
DOI: 10.1039/c0nj00423e

Photocatalytic oxidation of cyclohexane (CHA) with molecular oxygen has been performed with hydrophobic Cr–Si mixed oxides as a catalyst under visible light irradiation ($\lambda > 400$ nm). The Cr–Si catalysts with highly dispersed chromate species were prepared by hydrolysis of tetraethyl orthosilicate (TEOS), organoalkoxysilane (1,2-bis(triethoxysilyl)ethane: BTESE), and $Cr(NO_3)_3$ followed by calcination. All of the Cr–Si catalysts promote partial oxidation of CHA to cyclohexanol (CHA-ol) and cyclohexanone (CHA-one) with high selectivity (>99%). Among the Cr–Si catalysts prepared with different TEOS and BTESE compositions, the catalyst prepared with 10% BTESE demonstrates the highest catalytic activity. The CHA vapor adsorption and electron spin resonance analysis reveal that the enhanced catalytic activity is due to the increased hydrophobicity of the catalyst surface, which enhances the access of CHA to the excited state chromate species.

1. Introduction

The partial oxidation of cyclohexane (CHA) to cyclohexanol (CHA-ol) and cyclohexanone (CHA-one) has attracted much attention because these products are the intermediates in ε-caprolactam synthesis.[1] Of particular interest is the catalytic CHA oxidation in heterogeneous systems with molecular oxygen (O_2) as an oxidant.[2] Photocatalytic CHA oxidation in liquid/solid heterogeneous systems with O_2 has also been studied extensively with various catalysts such as TiO_2,[3] Fe porphyrin-modified TiO_2,[4] polyoxotungstate-modified SiO_2,[5] and V_2O_5-impregnated Al_2O_3.[6] Some of these systems promote partial oxidation of CHA with very high selectivity (>98%).[3b,f,g,4a,5] All of these systems, however, require UV light for catalyst activation.

Earlier, we reported a new photocatalytic CHA oxidation process with Cr–Si binary oxide catalysts (Cr–Si catalysts), prepared by hydrolysis of tetraethyl orthosilicate (TEOS) and $Cr(NO_3)_3$ followed by calcination.[7] The Cr–Si catalysts containing highly dispersed chromate species promote partial oxidation of CHA to CHA-ol and CHA-one with high selectivity (>99%) in a MeCN/catalyst heterogeneous system under irradiation of visible light ($\lambda > 400$ nm).[7]

The rate of catalytic reactions in heterogeneous systems depends on the surface hydrophobicity of catalysts because the surface hydrophobicity strongly affects the affinity of reactant with catalytic active site.[8] Silica materials are basically hydrophilic due to a large number of surface silanol groups,[9] while CHA is hydrophobic. The rate of CHA oxidation would therefore be improved by an increase in the surface hydrophobicity of catalyst. The surface of silica materials can easily be made hydrophobic by an introduction of hydrophobic organic fragments. These organosilicas are synthesized by two principal ways such as post-synthesis[10] and direct synthesis.[11] The former consists of a reaction of solid silica materials with an organochloro- or organoalkoxysilanes, where the organic fragments are anchored on the material surface. The latter consists of a hydrolysis of TEOS and organosilanes such as 1,2-bis(triethoxysilyl)ethane (BTESE). In the latter method, organic fragments are homogeneously introduced into the silica framework, and a larger amount of organic fragments are incorporated in the materials than with the former method. In addition, the surface hydrophobicity is easily controlled by changing the composition of TEOS and BTESE. Furthermore, the materials, when calcined at high temperature, still show high surface hydrophobicity, even though the organic fragments are completely decomposed.[12]

The purpose of the present work is to improve the rate of CHA oxidation, while maintaining high oxidation selectivity. We prepared hydrophobic Cr–Si catalysts by a hydrolysis of TEOS, BTESE, and $Cr(NO_3)_3$ followed by calcination. We hypothesized that the hydrophobic catalyst surface enhances the access of hydrophobic CHA to the photoexcited chromate species and improve the catalytic activity. We used four kinds of Cr–Si(x) catalysts prepared with different BTESE compositions [x (mol%) = BTESE/(BTESE + TEOS) × 100; x = 5, 10, 20, and 50] and studied the effects of organic modification on the catalytic activity and selectivity. We found that Cr–Si(10) catalyst prepared with 10% BTESE shows the activity twofold higher than that of Cr–Si(0) prepared without BTESE,[7] while maintaining high selectivity. The CHA vapor adsorption and ESR analysis were carried out to clarify the mechanism for oxidation enhancement on the Cr–Si(10) catalyst.

Research Center for Solar Energy Chemistry, and Division of Chemical Engineering, Graduate School of Engineering Science, Osaka University, Toyonaka 560-8531, Japan.
E-mail: shiraish@cheng.es.osaka-u.ac.jp; Fax: +81 6-6850-6273; Tel: +81 6-6850-6271

† Electronic supplementary information (ESI) available: N_2 adsorption and desorption isotherm of *pg*-Cr–Si(x) and Cr–Si(x) (Fig. S1). See DOI: 10.1039/c0nj00423e

2. Experimental

2.1 Materials

All of the reagents were supplied from Wako, Tokyo Kasei, and Sigma-Aldrich and used without further purification. Water was purified by the Milli Q system. JRC-TIO-4 TiO_2 particles (equivalent to Degussa P25) were supplied from the Catalysis Society of Japan and used as a reference catalyst.

2.2 Preparation of Cr–Si(*x*) catalysts

Five kinds of Cr–Si(*x*) catalysts [*x* (mol%) = BTESE/(BTESE + TEOS) × 100; *x* = 0, 5, 10, 20, and 50] were prepared by calcination of the corresponding precursor gels, *pg*-Cr–Si(*x*), according to the procedure described previously,[7] as follows: in a typical synthesis for *x* = 10, TEOS (45 mmol; 9.76 g), BTESE (5 mmol; 1.84 g), and $Cr(NO_3)_3{\cdot}9H_2O$ (0.05 mmol; 0.02 g) were dissolved in ethylene glycol (8.4 g) and stirred at 363 K for 3 h. Water (40 g) was added to the mixture and stirred at 363 K for 5 h. The resultant was dried at 383 K for 12 h, affording a green-white powder of the precursor gel, *pg*-Cr–Si(10). The gel was calcined at 773 K for 5 h under air affording a yellow-white powder of Cr–Si(10). The properties of *pg*-Cr–Si(*x*) and Cr–Si(*x*) are summarized in Tables 1 and 2, respectively.

2.3 Photoreaction

The respective catalysts (50 mg) were added to MeCN (9 mL) containing CHA (1 mL) within a Pyrex glass tube (20 cm^3; ϕ = 10 mm), and the tube was sealed using a rubber septum cap. O_2 gas was bubbled through the solution for 5 min at 273 K. Each tube was photoirradiated with magnetic stirring by a Xe lamp (2 kW; Ushio Inc.),[13] filtered through an aqueous $NaNO_2$ (3 wt%) solution[14] to give light wavelengths of $\lambda > 400$ nm. The solution temperature during photoirradiation was 313 K, and the light intensity was 16.0 mW m^{-2} (at 400–530 nm; through the $NaNO_2$ filter). After photoirradiation, the gas phase product was analyzed by GC-TCD (Shimadzu; GC-8A). The resulting solution was recovered by centrifugation and analyzed by GC-FID (Shimadzu; GC-1700), where the product identifications were made by GC-MS (EI) (Shimadzu; GCMS-QP5050A).

Table 1 Properties of the precursor gels, *pg*-Cr–Si(*x*)

	Cr (mol%)[a]	S_{BET}[b]/m^2 g^{-1}	V_p[c]/mm^3 g^{-1}	D_p[d]/nm
pg-Cr–Si(0)	0.076	789	684	3.5
pg-Cr–Si(5)	0.077	764	629	3.3
pg-Cr–Si(10)	0.077	748	583	3.1
pg-Cr–Si(20)	0.078	734	514	2.8
pg-Cr–Si(50)	0.072	675	477	2.8

[a] = Cr/(Cr + Si) × 100. [b] BET surface area determined by N_2 adsorption–desorption data (Fig. S1, ESI†). [c] Total pore volume. [d] Average pore diameter ($=4V_p/S_{BET}$).

2.4 ESR measurement

The spectra were recorded at the X-band using a Bruker EMX-10/12 spectrometer with a 100 kHz magnetic field modulation at a microwave power level of 1.0 mW,[15] where microwave power saturation of the signals does not occur. The magnetic field was calibrated using a 1,1′-diphenyl-2-picrylhydrazyl (DPPH) as standard. Catalyst (50 mg) was placed in a quartz ESR tube and treated with 100 Torr oxygen (1 Torr = 133.3 Pa) at 673 K for 1 h. The tube was then evacuated at 473 K for 2 h and cooled to room temperature. Required quantity of O_2 or CHA was introduced to the tube. The tube was placed on an ESR sample cavity and photoirradiated at 77 K using a 500 W Xe lamp (USHIO Inc.). After 0.5 h of photoirradiation, measurement was started with continued photoirradiation.

2.5 Other analysis

The Cr content of the catalyst was analyzed by an inductively-coupled argon plasma atomic emission spectrophotometer (Nippon Jarrell-Ash; ICAP575 Mark II) after washing with HF.[16] BET surface area and pore size distribution of the catalysts were determined by N_2 adsorption–desorption analysis at 77 K using a BELSORP 18PLUS-SP analyzer (BEL Japan, Inc.). The CHA monolayer adsorption capacity per unit surface area of catalysts (q_{CHA}) was determined by the vapor adsorption measurement at 298 K using the BELSORP system. Diffuse reflectance UV-vis spectra of the catalysts were measured on a UV-vis spectrophotometer (Jasco Corp.; V-550 with Integrated Sphere Apparatus ISV-469) using $BaSO_4$ as reference. IR spectra were measured using an FT-IR-610 infrared spectrophotometer (Jasco Corp.). Particle size distribution was determined using a Horiba LA-910 laser light-scattering particle size analyzer.

3. Results and discussion

3.1 Synthesis and properties of catalysts

The Cr–Si(*x*) catalysts [*x* (mol%) = BTESE/(BTESE + TEOS) × 100; *x* = 0, 5, 10, 20, and 50] were synthesized by calcination of the precursor gels, *pg*-Cr–Si(*x*), prepared by

Table 2 Properties of Cr–Si(*x*) catalysts

	Cr (mol%)[a]	S_{BET}[b]/m^2 g^{-1}	V_p[c]/mm^3 g^{-1}	D_p[d]/nm	Particle size[e]/μm	V_m[f]/mmol g^{-1}	q_{CHA}[g]/molecules nm^{-2}
Cr–Si(0)	0.076	804	729	3.6	71.5	2.04	1.53
Cr–Si(5)	0.084	769	522	2.7	63.7	2.52	1.97
Cr–Si(10)	0.080	608	452	3.0	62.7	2.18	2.16
Cr–Si(20)	0.084	557	351	2.5	63.0	1.70	1.84
Cr–Si(50)	0.077	316	213	2.7	71.7	0.91	1.73

[a] = Cr/(Cr + Si) × 100. [b] BET surface area determined by N_2 adsorption–desorption data (Fig. S1, ESI†). [c] Total pore volume. [d] Average pore diameter ($=4V_p/S_{BET}$). [e] Determined by static laser scattering analysis. [f] Monolayer adsorption capacity of CHA (p/p_0 = 0.10–0.30). [g] Adsorption capacity of CHA per unit surface area = $(V_m/10^3) \times (10^{-18}/S_{BET}) \times N$ (N = Avogadro's number).

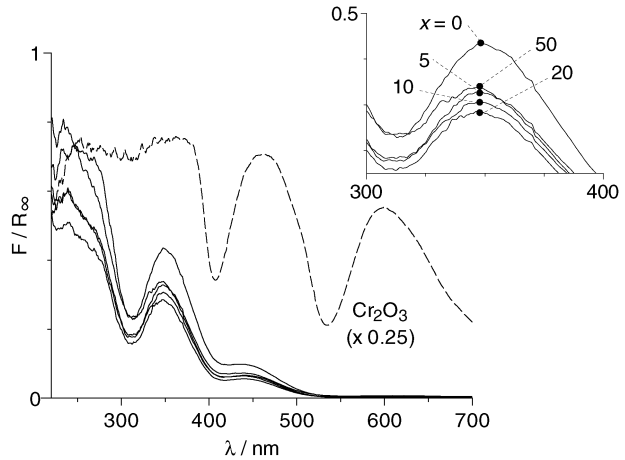

Fig. 1 UV-vis diffuse reflectance spectra of Cr–Si(x) and Cr_2O_3.

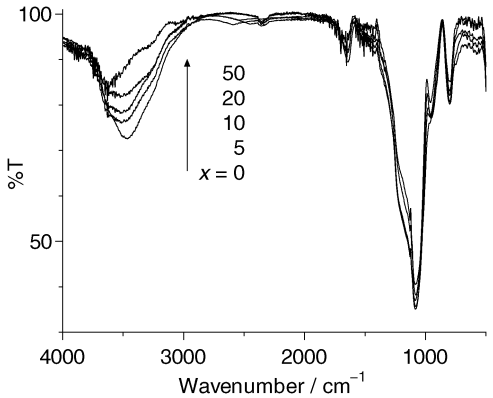

Fig. 2 IR spectra of Cr–Si(x).

hydrolysis of TEOS, BTESE, and $Cr(NO_3)_3$. The properties of the precursor gels and catalysts are summarized in Tables 1 and 2, respectively. As shown in Table 2, all of the Cr–Si(x) catalysts contain 0.075–0.085 mol% Cr. Fig. 1 shows the UV-vis diffuse reflectance spectra of the catalysts. These catalysts show three distinctive absorption bands centered at 250, 350 and 450 nm, assigned to a ligand-to-metal charge transfer (LMCT) band from O^{2-} to Cr^{6+} transitions of the chromate species, which are highly dispersed on silica matrices and isolated from each other.[17] In contrast, bulk Cr_2O_3 shows red-shifted absorption band at 500–800 nm (dotted line), assigned to a d–d transition of the octahedral Cr^{3+} species in a Cr_2O_3 cluster.[17] Such red-shifted absorption is not observed for Cr–Si(x) catalysts, indicating that these Cr–Si(x) catalysts contain highly dispersed chromate species.

Table 2 (final column) summarizes the CHA monolayer adsorption capacity per unit surface area of the catalysts (q_{CHA}) determined by the CHA vapor adsorption analysis. The q_{CHA} values of Cr–Si(x) (x = 5, 10, 20, 50) are >1.73, which are higher than that of Cr–Si(0) (1.53). This indicates that the surface hydrophobicity of catalysts prepared with BTESE are indeed higher than that prepared without BTESE, even after the ethane fragments are removed by calcination, as observed for related materials.[12a] This is due to the condensation of silanol (Si–OH) groups. During calcination, decomposition of ethane fragments (Si–C cleavage) leads to a sequential reaction between the resulting Si atom and the adjacent silanol group, forming a siloxane (Si–O–Si) group.[18] Fig. 2 shows IR spectra of the catalysts. The Si–OH absorption observed at *ca.* 3500 cm^{-1} decreases with an increase in the BTESE amount in the precursor gel. This indicates that the removal of ethane fragments by calcination leads to a silanol condensation and, hence, results in an increase in surface hydrophobicity of the catalysts.

3.2 Photocatalytic properties

Photocatalytic oxidation of CHA with O_2 was carried out with Cr–Si(x) catalysts. Table 3 summarizes the yields of CO_2 and partially-oxidized (PO) products (CHA-one and CHA-ol) obtained by visible light irradiation (λ >400 nm) for 5 h by a Xe lamp. As shown in runs 1–5, all Cr–Si catalysts promote CHA oxidation under visible light irradiation. As shown in run 6, a bulk Cr_2O_3 does not promote oxidation. This suggests that, as described previously,[7] the polymerized Cr^{3+} species are inactive, and the highly dispersed chromate species are the active species.

As shown in runs 1–5, Cr–Si(x) prepared with BTESE shows high PO product selectivity (>99%), as does Cr–Si(0) prepared without BTESE. This indicates that the increased

Table 3 Results of photocatalytic oxidation of cyclohexane (CHA) under visible light irradiation[a]

Run	Catalyst	Yields/μmol			PO product selectivity[c] (%)	TON[d]
		CHA-one	CHA-ol	CO_2[b]		
1	Cr–Si(0)	5.9	3.0	<0.2	>99	14
2	Cr–Si(5)	9.1	4.0	<0.2	>99	19
3	Cr–Si(10)	10.2	4.2	1.3	99	22
4	Cr–Si(20)	5.7	2.8	0.5	99	12
5	Cr–Si(50)	4.4	2.1	0.2	99	10
6	Cr_2O_3[e]	N.D.	N.D.	N.D.		
7	TiO_2[e]	3.7	1.9	11.0	50	
8	Cr–Si(10)[f]	10.0	3.8	1.0	99	22
9	Cr–Si(10)[g]	9.8	3.9	1.1	99	21
10	Cr–Si(10)[h]	1.0	0.9	0.3	97	4

[a] Reaction conditions: catalyst, 50 mg; MeCN, 9 mL; CHA, 1 mL; O_2, 1 atm; photoirradiation time, 5 h; >400 nm. [b] Detection limit is 0.2 μmol. [c] =[(CHA-one + CHA-ol)/(CHA-one + CHA-ol + (1/6)CO_2)] × 100 (ref. 5). [d] =[(CHA-one yields) + (CHA-ol yields)]/(Cr amount on the catalyst). [e] Catalyst, 10 mg. [f] After the reaction (run 3), the catalyst was recovered by filtration and washed with MeCN, and used for reaction. [g] 2nd reuse. [h] Without MeCN (10 mL CHA was used for reaction).

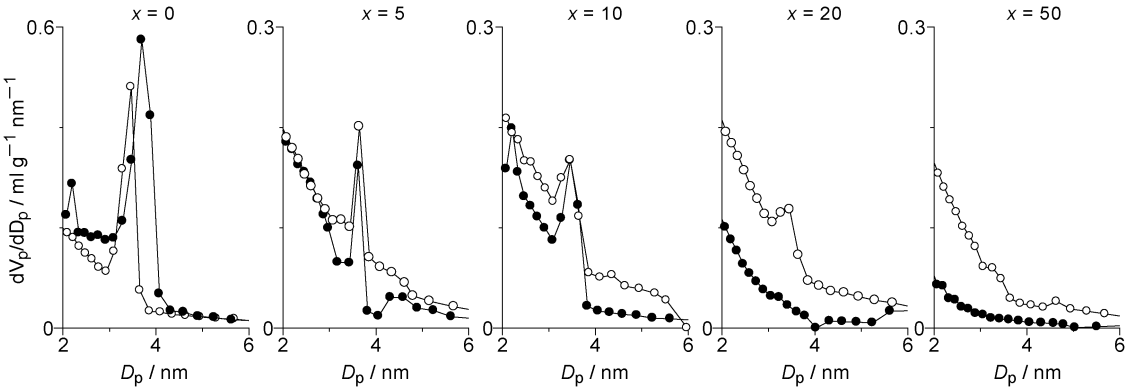

Fig. 3 Pore size distribution of (open keys) *pg*-Cr–Si(x) and (closed keys) Cr–Si(x).

surface hydrophobicity of the catalysts scarcely affects the oxidation selectivity. As shown in run 7, a common TiO_2 photocatalyst (JRC-TIO-4; equivalent to Degussa P25) shows a selectivity (50%) much lower than that of Cr–Si catalysts. These data suggest that the Cr–Si(x) systems promote selective oxidation of CHA under visible light irradiation. It must be noted that the catalyst is reusable for further reaction. After the reaction with Cr–Si(10) (run 3), the catalyst was recovered by filtration. ICP analysis of the resulting solution does not detect Cr leaching. In addition, as shown in runs 8 and 9, the recovered catalyst, when reused for further CHA oxidation, shows almost the same activity and PO product selectivity as does the virgin catalyst (run 3). The data indicate that the catalyst is reusable without loss of activity and selectivity.

3.3 Photocatalytic activity

Table 3 (final column) summarizes the change in turnover number (TON) for PO product formation [=(amount of PO products formed)/(amount of Cr on the catalyst)] during 5 h photoirradiation. The TON values increase with an increase in the BTESE amount in the precursor gel; the value of Cr–Si(0) is 14, whereas that of Cr–Si(5) and (10) catalysts are 19 and 22, respectively. The increased catalytic activity is due to the enhanced access of CHA to the photoexcited chromate species on the catalyst surface. As shown in Table 2 (final column), the CHA monolayer adsorption capacity per unit surface area (q_{CHA}) of Cr–Si(5) and (10) catalysts are higher than that of Cr–Si(0). This indicates that a larger quantity of CHA is adsorbed onto the hydrophobic surface of the catalysts; in other words, the chromate species are surrounded by a larger quantity of CHA. This therefore enhances the access of CHA to photoexcited chromate species, resulting in an acceleration of CHA oxidation on the Cr–Si(5) and (10) catalysts.

As shown in Table 3, the TON values of Cr–Si(20) and (50) are much lower than that of Cr–Si(10), although these catalysts are prepared with larger amount of BTESE. This is because calcination of the precursor gel prepared with larger amount of BTESE leads to a shrinkage of silica framework and produces plugged pores, which suppresses the access of CHA to the chromate species. As shown in Table 1 (second column), the surface area of the precursor gels (*pg*-Cr–Si(x)) prepared with different BTESE amount are similar to each other (670–780 $m^2\ g^{-1}$). As shown in Table 2 (second column), Cr–Si(x) have a smaller surface area than the corresponding *pg*-Cr–Si(x). In particular, Cr–Si(x) prepared with larger BTESE amount shows a significant decrease in the surface area. This indicates that the shrinkage of silica framework actually occurs during the removal of ethane fragments by calcination. Fig. 3 shows the pore size distribution of *pg*-Cr–Si(x) and Cr–Si(x). The Cr–Si(x) prepared with larger BTESE amount shows much broader pore distribution than the corresponding *pg*-Cr–Si(x). These data clearly indicate that the Cr–Si(x) prepared with larger amount of BTESE has a constricted structure and contains plugged pores. In such case, the CHA molecules cannot access the chromate species confined within the plugged pores. This probably results in very low catalytic activity on the Cr–Si(20) and (50) catalysts. The pore plugging is supported by the CHA adsorption capacity data. As shown in Table 2 (final column), the q_{CHA} values of Cr–Si(20) and (50) are much lower than that of Cr–Si(10). This is because the plugged pores suppress the CHA adsorption.

3.4 Properties of photoexcited chromate species

The properties of chromate species on the Cr–Si(x) catalysts were studied by ESR analysis. The structure and catalytic mechanism of Cr–Si(0) have been described in our previous work,[7] as shown in Scheme 1. Fig. 4.i (bold line) shows the ESR spectra of Cr–Si(0), (10), and (50) catalysts measured *in vacuo* at 77 K. The spectra consist of two major signals, assigned to the reduced tetrahedral ($T_d{}^{5+}$; $g_\perp$ = 1.975, $g_\parallel$ = 1.960) and square-pyramidal ($S_p{}^{5+}$; $g_\perp$ = 1.987, $g_\parallel$ = 1.900) species.[19] The S_p species scarcely form excited state and T_d species act as the active site for oxidation.[7] This is confirmed by photoirradiation of the samples: as shown in Fig. 4.i (normal line), photoirradiation leads to a decrease in the $T_d{}^{5+}$ signal, while the $S_p{}^{5+}$ signal scarcely changes. The $T_d{}^{5+}$ signal decrease on these samples is due to the photo-reduction of Cr^{5+} to Cr^{4+} (formation of $T_d{}^{4+}$* species). The formation of Cr^{3+} and Cr^{2+} species can be ruled out because distinctive Cr^{3+} signal does not appear in the absence and presence of O_2.[19] This indicates that the $T_d{}^{4+}$* species acts as the active site for these samples. The photoexcitation mechanism of chromate species on Cr–Si(10) and (50) catalysts is therefore explained with that of Cr–Si(0):[7] as shown in Scheme 1a, the catalyst prepared with a sol–gel method contains Cr species

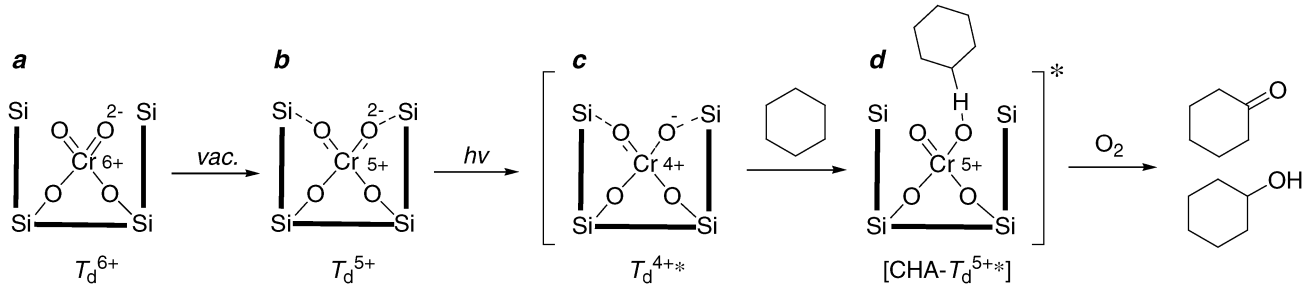

Scheme 1 Photocatalysis mechanism of chromate species on Cr–Si(0) and (10) catalysts.

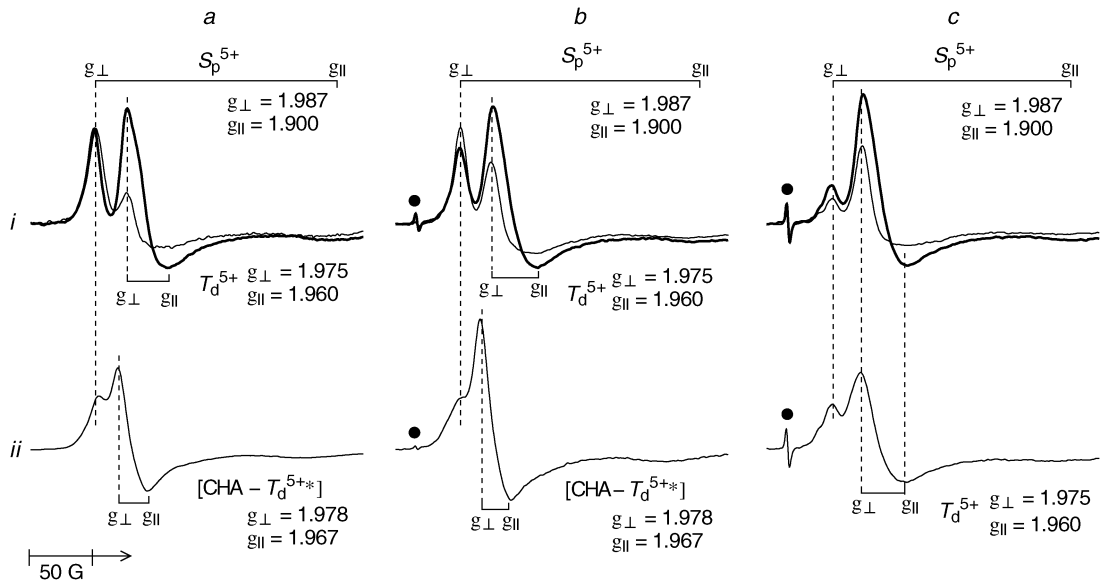

Fig. 4 ESR spectra (77 K) of (a) Cr–Si(0), (b) Cr–Si(10), and (c) Cr–Si(50) catalysts, when measured (i) *in vacuo* (bold) without photoirradiation and (normal) with photoirradiation and measured (ii) with photoirradiation in the presence of 1 Torr CHA. The signal indicated by closed circle symbol (g = 2.003) is assigned to the carbonaceous residues derived from BTESE.

arranged homogeneously with Si species. The reduction of T_d^{6+} to T_d^{5+} *in vacuo* occurs due to a terminal oxygen (O_T)–Si bond formation associated with H_2O removal from the adjacent Si species.[20] On the stabilized T_d^{5+} species, photoinduced charge transfer between O_T and Cr occurs easily, thus promoting a formation of T_d^{4+}* species (Scheme 1c).

Fig. 4a and b.ii show the ESR spectra of Cr–Si(0) and (10) obtained with CHA (1 Torr) under photoirradiation at 77 K. A new T_d^{5+}* signal ($g_\perp$ = 1.978; $g_\parallel$ = 1.967) appears on both samples. The O_T formed by photoinduced electron transfer has an electrophilic character and acts as a positive hole.[21] The new T_d^{5+}* signal is assigned to the [CHA–T_d^{5+}*] complex formed *via* a H attraction by the electrophilic O_T on T_d^{4+}* (Scheme 1d), which leads to oxidation of Cr^{4+} to Cr^{5+}.[7] The CHA oxidation on Cr–Si(10) therefore proceeds *via* a reaction of this complex with O_2, as is the case for Cr–Si(0) (Scheme 1d). It must be noted that the intensity of [CHA–T_d^{5+}*] signal on Cr–Si(10) is larger than that on Cr–Si(0). This indicates that the T_d^{4+}* species on Cr–Si(10) reacts efficiently with CHA and produces larger quantity of [CHA–T_d^{5+}*] complex. This is because the access of CHA to the T_d^{4+}* species is enhanced on the hydrophobic surface of Cr–Si(10). The result agrees with the q_{CHA} values of Cr–Si(10) higher than that of Cr–Si(0). This clearly suggests that the enhanced access of CHA to the hydrophobic surface of Cr–Si(10) promotes efficient CHA oxidation (Table 3).

As shown in Table 3, Cr–Si(50) shows catalytic activity much lower than Cr–Si(10). The surface area and q_{CHA} data (Table 2) suggest that the decreased activity of Cr–Si(50) is due to the pore plugging by calcination, which suppresses the CHA access to the T_d^{4+}* species. This is confirmed by ESR analysis with Cr–Si(50). As shown in Fig. 4c.i, the spectra obtained *in vacuo* without and with photoirradiation are similar to that of Cr–Si(0) and (10), indicating that, on Cr–Si(50), T_d^{4+}* is also produced by photoirradiation. As shown in Fig. 4a and b.ii, photoirradiation of Cr–Si(0) and (10) with CHA produces a [CHA–T_d^{5+}*] signal. However, as shown in Fig. 4c.ii, Cr–Si(50) scarcely shows the [CHA–T_d^{5+}*] signal, where the T_d^{5+}* signal still remains even after the CHA addition. This indicates that, on Cr–Si(50), the reaction of CHA with T_d^{4+}* is suppressed strongly. The results again suggest that the plugged pores on Cr–Si(50) suppress the CHA access to the T_d species, resulting in low catalytic activity of Cr–Si(50).

It must be noted that, in the present process, the solvent MeCN is important for catalytic activity. As shown in Table 3 (run 10), the product yields during reaction in pure CHA are

much lower than that obtained with MeCN (run 3). One of the possible reasons for this effect is the stability enhancement of the T_d^{4+}* species in polar MeCN. This is supported by ESR analysis. As shown in Fig. 4.i, the T_d^{5+} spectra for Cr–Si(0), (10), and (50) catalysts obtained *in vacuo* are similar. Photo-irradiation of the catalysts leads to an intensity decrease due to the formation of T_d^{4+}* species. The intensity decrease becomes smaller with an increase in the BTESE content of the catalysts, indicating that the quantity of T_d^{4+}* decreases with the BTESE content increase. The T_d^{4+}* species has a charge-transferred electronic structure.[21] The decreased T_d^{4+}* quantity is probably because the T_d^{4+}* species is destabilized by hydrophobic surface of the catalyst. Addition of polar MeCN to the solution probably stabilizes the T_d^{4+}* species as compared to the case with pure CHA. This may be the reason for the activity improvement by the MeCN addition.

4. Conclusion

Hydrophobic Cr–Si(x) catalysts containing highly dispersed chromate species were synthesized by a hydrolysis of TEOS, BTESE, and Cr salts. These catalysts were used for CHA oxidation with O_2 under visible light irradiation. All Cr–Si(x) catalysts promote partial CHA oxidation with high selectivity. Among the catalysts, Cr–Si(10) prepared with 10% BTESE shows the highest catalytic activity. The enhanced activity of Cr–Si(10) than that of Cr–Si(0) prepared without BTESE is due to the increase in surface hydrophobicity of the catalyst, which accelerates the reaction of CHA with the excited state chromate species (T_d^{4+}*). In contrast, Cr–Si(x) prepared with $>20\%$ BTESE shows the decreased activity. This is because the calcination of precursor gel leads to a shrinkage of the pores. This suppresses the access of CHA to the T_d^{4+}* species confined within the plugged pores.

Acknowledgements

This work was supported by the Grant-in-Aid for Scientific Research (No. 19760536) from the Ministry of Education, Culture, Sports, Science and Technology, Japan (MEXT). H.O. thanks the Japan Society of Promotion of Science (JSPS) Research Fellowships for Young Scientist.

Notes and references

1 (*a*) U. Schuchardt, D. Cardoso, R. Sercheli, R. Pereira, R. S. da Cruz, M. C. Guerreiro, D. Mandelli, E. V. Spinacé and E. L. Pires, *Appl. Catal., A*, 2001, **211**, 1–17; (*b*) G. Bellussi and C. Perego, *CATTECH*, 2000, **4**, 4–16; (*c*) A. Castellan, J. C. J. Bart and S. Cavallaro, *Catal. Today*, 1991, **9**, 237–254.
2 (*a*) R. Zhao, D. Ji, G. Lv, G. Qian, L. Yan, X. Wang and J. Suo, *Chem. Commun.*, 2004, 904–905; (*b*) R. Raja, G. Sankar and J. M. Thomas, *J. Am. Chem. Soc.*, 1999, **121**, 11926–11927.
3 (*a*) C. Giannotti, S. Le Greneur and O. Watts, *Tetrahedron Lett.*, 1983, **24**, 5071–5072; (*b*) G. Lu, H. Gao, J. Suo and S. Li, *J. Chem. Soc., Chem. Commun.*, 1994, 2423–2424; (*c*) P. Boarini, V. Carassiti, A. Maldotti and R. Amadelli, *Langmuir*, 1998, **14**, 2080–2085; (*d*) A. Sclafani and J. M. Herrmann, *J. Phys. Chem.*, 1996, **100**, 13655–13661; (*e*) K.-I. Shimizu, T. Kaneko, T. Fujishima, T. Kodama, H. Yoshida and Y. Kitayama, *Appl. Catal., A*, 2002, **225**, 185–191; (*f*) C. B. Almquist and P. Biswas, *Appl. Catal., A*, 2001, **214**, 259–271; (*g*) M. A. Brusa and M. A. Grela, *J. Phys. Chem. B*, 2005, **109**, 1914–1918; (*h*) M. A. Gonzalez, S. G. Howell and S. K. Sikdar, *J. Catal.*, 1999, **183**, 159–162.
4 (*a*) R. Amadelli, M. Bregola, E. Polo, V. Carassiti and A. Maldotti, *J. Chem. Soc., Chem. Commun.*, 1992, 1355–1357; (*b*) A. Molinari, R. Amadelli, L. Antolini, A. Maldotti, P. Battioni and D. Mansuy, *J. Mol. Catal. A: Chem.*, 2000, **158**, 521–531.
5 (*a*) A. Molinari, R. Amadelli, L. Andreotti and A. Maldotti, *J. Chem. Soc., Dalton Trans.*, 1999, 1203–1204; (*b*) A. Maldotti, A. Molinari, G. Varani, M. Lenarda, L. Storaro, F. Bigi, R. Maggi, A. Mazzacani and G. Sartori, *J. Catal.*, 2002, **209**, 210–216.
6 (*a*) K. Teramura, T. Tanaka, T. Yamamoto and T. Funabiki, *J. Mol. Catal. A: Chem.*, 2001, **165**, 299–301; (*b*) K. Teramura, T. Tanaka, M. Kani, T. Hosokawa and T. Funabiki, *J. Mol. Catal. A: Chem.*, 2004, **208**, 299–305.
7 (*a*) Y. Shiraishi, Y. Teshima and T. Hirai, *Chem. Commun.*, 2005, 4569–4571; (*b*) Y. Shiraishi, Y. Teshima and T. Hirai, *J. Phys. Chem. B*, 2006, **110**, 6257–6263.
8 (*a*) A. Corma, P. Esteve and A. Martínez, *J. Catal.*, 1996, **161**, 11–19; (*b*) M. A. Camblor, A. Corma, P. Esteve, A. Martínez and S. Valencia, *Chem. Commun.*, 1997, 795–796.
9 T. Blasco, A. Corma, M. T. Navarro and J. P. Pariente, *J. Catal.*, 1995, **156**, 65–74.
10 (*a*) K. A. Koyano, T. Tatsumi, Y. Tanaka and S. Nakata, *J. Phys. Chem. B*, 1997, **101**, 9436–9440; (*b*) A. Corma, M. Domine, J. A. Gaona, J. L. Jordá, M. T. Navarro, F. Rey, J. Pérez-Pariente, J. Tsuji, B. McCulloch and L. T. Nemeth, *Chem. Commun.*, 1998, 2211–2212.
11 (*a*) T. Asefa, M. J. MacLachlan, N. Coombs and G. A. Ozin, *Nature*, 1999, **402**, 867–871; (*b*) S. Inagaki, S. Guan, Y. Fukushima, T. Ohsuna and O. Terasaki, *J. Am. Chem. Soc.*, 1999, **121**, 9611–9614.
12 (*a*) A. Bhaumik, M. P. Kapoor and S. Inagaki, *Chem. Commun.*, 2003, 470–471; (*b*) M. P. Kapoor, A. Bhaumik, S. Inagaki, K. Kuraoka and T. Yazawa, *J. Mater. Chem.*, 2002, **12**, 3078–3083.
13 Y. Shiraishi, Y. Sugano, S. Tanaka and T. Hirai, *Angew. Chem., Int. Ed.*, 2010, **49**, 1656–1660.
14 Y. Shiraishi, N. Saito and T. Hirai, *Chem. Commun.*, 2006, 773–775.
15 Y. Shiraishi, N. Saito and T. Hirai, *J. Am. Chem. Soc.*, 2005, **127**, 8304–8306.
16 Y. Shiraishi, M. Morishita, Y. Teshima and T. Hirai, *J. Phys. Chem. B*, 2006, **110**, 6587–6594.
17 (*a*) T. Kamegawa, J. Morishima, M. Matsuoka, J. M. Thomas and M. Anpo, *J. Phys. Chem. C*, 2007, **111**, 1076–1078; (*b*) F. Amano, T. Yamaguchi and T. Tanaka, *J. Phys. Chem. B*, 2006, **110**, 281–288.
18 M. Morishita, Y. Shiraishi and T. Hirai, *J. Phys. Chem. B*, 2006, **110**, 17898–17905.
19 (*a*) B. M. Weckhuysen, I. E. Wachs and R. A. Schoonheydt, *Chem. Rev.*, 1996, **96**, 3327–3349; (*b*) B. M. Weckhuysen, A. A. Verberckmoes, A. L. Buttiens and R. A. Schoonheydt, *J. Phys. Chem.*, 1994, **98**, 579–584.
20 B. M. Weckhuysen, R. A. Schoonheydt, J.-M. Jehng, I. E. Wachs, S. J. Cho, R. Ryoo, S. Kijlstra and E. Poels, *J. Chem. Soc., Faraday Trans.*, 1995, **91**, 3245–3253.
21 K. Wada, H. Yamada, Y. Watanabe and T. Mitsudo, *J. Chem. Soc., Faraday Trans.*, 1998, **94**, 1771–1778.

